08,03

Microwave Optical Spectroscopy of Polyvalent Charge States of Transition Element Ions in Silicon Carbide

© R.A. Babunts, D.D. Kramushchenko, Yu.A. Uspenskaya, I.V. Ilyin, A.P. Bundakova, M.V. Muzafarova¶, P.G. Baranov

Ioffe Institute,
St. Petersburg, Russia

¶ E-mail: marina.muzafarova@mail.ioffe.ru

Received August 8, 2023
Revised August 8, 2023
Accepted August 16, 2023

Four possible charge states of molybdenum in silicon carbide (SiC) are analyzed: paramagnetic $Mo^{3+}(4d^3)$, $Mo^{4+}(4d^2)$, $Mo^{5+}(4d^1)$, characterized by axial symmetry, and diamagnetic $Mo^{6+}(4d^0)$. Using high-frequency electron paramagnetic resonance (EPR) and low temperatures for Mo^{4+} with spin $S = 1$, which is the neutral charge state in the A^0 crystal, a positive sign of the fine structure splitting D was established for two quasi-cubic positions k1 and k2: $D(\text{k1}) = 3.06\,\text{GHz}$, $D(\text{k2}) = 3.29\,\text{GHz}$ and the values of g-factor are determined: $g_{\parallel} = 1.9787$ and $g_{\perp} = 1.9811$, that is, $g_{\perp} > g_{\parallel}$. The contributions of paramagnetic and diamagnetic components in non-phonon lines of optical absorption of Mo^{4+} ions in the near-IR region were separated by magnetic circular dichroism (MCD) of absorption at different temperatures. For the charge state of $Mo^{5+}(4d^1)$, the off-center position of the substititional impurity in place of the silicon atom was established and superhyperfine (SHF) interactions with ligand nuclei ^{29}Si and ^{13}C were determined. A comparative analysis of hyperfine (HF) interactions with odd isotopes of molybdenum ^{95}Mo and ^{97}Mo having a nuclear magnetic moment in three charge states is carried out. Due to works using vanadium V^{4+} in SiC for quantum information and communication, since these defects have photoluminescence lines in the transmission window of about 1300 nm, it is shown that in the main transmission window of about 1540 nm, erbium Er^{3+} in SiC is very promising, and we previously managed to introduce Er^{3+} in SiC bulk crystals. It is important that at room temperature a significant decrease in the V^{4+} photoluminescence line in SiC is recorded, whereas for Er^{3+} ions in SiC such a decrease is insignificant and photoluminescence line can be observed up to 400 K.

Keywords: high-frequency electron paramagnetic resonance, magnetic circular dichroism of absorption, silicon carbide, molybdenum, vanadium, erbium, impurity centres.

DOI: 10.61011/PSS.2023.10.57227.175

1. Introduction

Recently, significant interest was shown in the study of the optical and spin properties of transition elements in silicon carbide (SiC), which we previously studied in a number of papers [1–7]. Spins associated with point intrinsic and impurity defects in SiC are considered as a platform for solid-state implementation of quantum light-matter interfaces in quantum information technology and spintronics. Such objects are currently vacancy spin centers of atomic size in diamond and SiC, which have optically addressable spin states, which makes them promising for quantum technologies, including the development of quantum memory on magnetic nuclei ^{29}Si and ^{13}C [6,8–13]. Recent studies demonstrated that transition metal ions in SiC may be promising for quantum applications, as they are characterized by emission in the near-infrared region, lying in the transparency band of fiber optics [14–16], while SiC is wide-band semiconductor material with well-developed technology.

A fully optical study of ensembles of molybdenum impurities in materials of p-types 4H-SiC and 6H-SiC was carried out in work [17]. In this paper it is assumed that Mo is in the charge state $Mo^{5+}(4d^1)$, i.e. four electrons of Mo are involved in bonds with SiC and the remaining electron in 4d-shell has a spin $S = 1/2$ for the ground and optically excited states and the observed photoluminescence (PL) in the near-infrared (IR) range is associated with this charge state. It is also proposed to use the anisotropy of the spin properties of molybdenum to implement optical control of spin coherence in the ground state, which is estimated as $\sim 0.3\,\mu$s, the lifetime in the excited state is ~ 60 ns. It is noted that knowledge about the spin and optical properties of transition metals in SiC is incomplete; however, the data obtained are not compared with the results of studies using EPR and ODMR methods previously carried out in papers [1–6].

The purpose of this paper is to analyze the paramagnetic and optical properties of various charge states of molybdenum, including consideration of hyperfine (HF) interactions with the nuclei of odd molybdenum isotopes, and superhyperfine (SHF) interactions with the nuclei of the ligands ^{29}Si and ^{13}C, located in the immediate environment of $Mo^{5+}(4d^1)$ ion, which is of main interest for applications [17]. High-frequency electron paramagnetic

resonance (EPR) methods will be used to study the unique properties of molybdenum centers in SiC in strong magnetic fields at low temperatures.

The property of transition elements to be in different charge states in SiC has a strong influence on the electrical characteristics of the material. The polyvalent properties of transition elements can be used to compensate for residual impurities of small donors or acceptors, resulting in that semiconductor material has semi-insulating properties, which is extremely important for the production of semi-insulating substrates required for high-power microwave devices. Effective compensation requires the presence of deep donor and acceptor levels inside the band gap. If the molybdenum concentration is higher than the uncompensated boron concentration, electrons from the molybdenum donor level will fill all boron acceptors. The excess electrons will remain in the molybdenum levels, anchoring the Fermi level at the middle of the band gap. Similar processes occur in the case of compensation of nitrogen donors, then electrons from nitrogen donors fill the acceptor levels of molybdenum if the molybdenum concentration is higher than the uncompensated nitrogen concentration.

Previous ESR studies [1–6] demonstrated that molybdenum has the mentioned polyvalent properties, since almost all possible charge states are realized, from Mo in the acceptor state, $Mo^{3+}(4d^3)$, neutral charged state, $Mo^{4+}(4d^2)$, donor state, $Mo^{5+}(4d^1)$, to the non-paramagnetic $Mo^{6+}(4d^0)$ state. The latter is confirmed by the complete disappearance of the EPR signals of molybdenum after the boron diffusion into SiC.

EPR spectra of the neutral state in SiC $Mo^{4+}(4d^2)$ with spin $S = 1$ were first recorded in the paper [7], but were attributed to isovalent chromium $Cr^{4+}(3d^2)$, as ions of another charge state of chromium $Cr^{3+}(3d^3)$ with a well-resolved hyperfine structure from the isotope ^{53}Cr (natural content 9.5%, nuclear spin $I = 3/2$) were simultaneously observed, at that due to the relatively weak EPR signal the HF structure was not observed in the EPR spectrum of the triplet center. Later, experiments with the same samples were repeated in papers [1–3], where it was possible to observe the HF structure of molybdenum for isotopes ^{95}Mo (natural content 15.9%) and ^{97}Mo (9.6%), nuclear spin for both isotopes $I = 5/2$. As a result, EPR signal in SiC was finally attributed to $Mo^{4+}(4d^2)$ ions. In the papers [1–3] EPR spectra of ions $Mo^{3+}(4d^3)$ with electron spin $S = 3/2$ and with well-resolved HF structure were also discovered. Thus, the three charge states of Mo were finally established.

2. Experiment procedure

In paper some types samples of samples of polytype 6*H*-SiC were used: i) epitaxial 6*H*-SiC layers grown by method of sublimation using Mo-crucible, sample No 1; ii) commercial samples of type No 2 and 3 in form of volume plates 6*H*-SiC *n*-type and *p*-type accordingly. Electron paramagnetic resonance (EPR) spectra were recorded in the standard *X*-range (9.4 GHz) and high-frequency *W*-range (94 GHz). High-frequency EPR makes it possible to observe the spectra of EPR centers with large splittings of the fine structure, exceeding the value of the microwave quantum in the standard EPR procedure, while the EPR spectra with large splittings of the fine structure are significantly simplified. Large magnetic fields and low temperatures make it possible to obtain high Boltzmann factors, which is important for determining the sign of the fine structure splitting, i. e., unambiguously establishing the structure of spin energy levels.

To obtain information about the excited electronic states of molybdenum impurity centers in 6*H*-SiC the magneto-optical studies were carried out in the near-IR spectral region. Magnetic circular dichroism (MCD) of absorption was recorded, which measures the difference in absorption for left-hand polarized (σ^+) and right hand polarized (σ^-) light ($I_{\sigma^+} - I_{\sigma^-}$) propagating along constant magnetic field in the sample. One of the disciplines of optical detection of magnetic resonance (ODMR) is the use of MCD, when changes in MCD absorption are recorded under EPR conditions in the ground state of the centers under study. Measuring the spectral dependence of magnetic resonance-induced changes in MCD absorption makes it possible to identify absorption bands of specific centers in complex spectra consisting of a number of bands, including overlapping optical absorption bands.

ODMR was registered by changes in MCD absorption at the moment of magnetic resonance at frequencies of 21, 35 and 94 GHz at temperature of 1.5 K and higher [18–20]. The magnetic field up to 6 T was created by a superconducting magnet. The light of a xenon or halogen lamp, isolated by a monochromator ($0.2-2\,\mu$m), or laser light was modulated by a quartz modulator $\pm\lambda/4$ (30 kHz) or by rotating mica plate $\lambda/4$ and after passing through the sample was registered by a photomultiplier. Signal $I_{\sigma^+} - I_{\sigma^-}$ signal is isolated by a synchronous detector. The total intensity $I = I_{\sigma^+} + I_{\sigma^-}$ was kept constant, which made it possible to observe the ODMR signal proportional to the MCD absorption value.

3. Results and results discussion

As mentioned above, we succeeded in identification of the EPR spectra of the three ground charge states of molybdenum in SiC. Figure 1 shows the crystal structure of 6*H*-SiC polytype and indicates the possible positions of the molybdenum impurity ion. In 6*H*-SiC there are three nonequivalent crystal positions: two quasicubic (k1, k2) and one hexagonal (h). The difference between the h position and two quasicubic positions k1 and k2 is due to the difference in the position of the atoms in the second coordination sphere; the difference between two quasicubic positions k1 and k2 appears when the third coordination sphere is also considered. Point group symmetry for all three positions — C_{3v}.

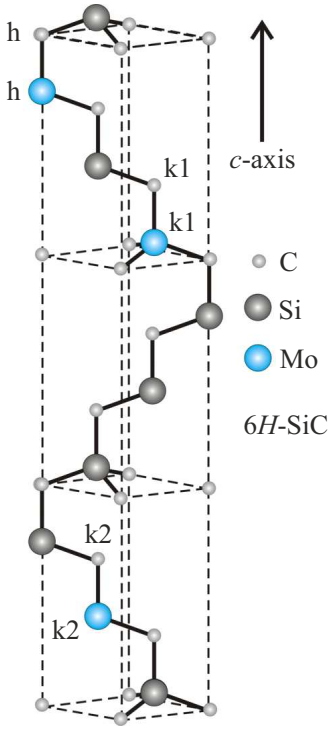

Figure 1. Crystal structure of 6*H*-SiC polytype, possible positions of the molybdenum impurity ion are indicated. In 6*H*-SiC there are three nonequivalent crystal positions: two quasicubic (k1, k2) and one hexagonal (h). Point group symmetry for all three positions — C_{3v}.

3.1. Molybdenum $Mo^{4+}(4d^2)$

3.1.1. Electron paramagnetic resonance

The tetravalent molybdenum ion $Mo^{4+}(4d^2)$ replaces silicon in SiC and represents a neutral charged state in the SiC crystal lattice. The ground electronic state of this ion $^3A_2$ is an electron triplet, $S = 1$. Figure 2, *a* shows the orientation dependence of the EPR spectra of $Mo^{4+}(4d^2)$ ions in compensated 6*H*-SiC crystal, registered in the sample No 1 at 4.5 K in the range 94 GHz, low-frequency modulation 680 Hz of magnetic field was used, the modulation amplitude was 0.2 mT. Intense signals of nitrogen donors are observed in the region $g \sim 2.0$ (the spectrum of ions Mn^{2+}, not related to SiC is visible). In a strong magnetic field at low temperatures the Boltzmann distribution of level populations is established, which makes it possible to determine the sign of the fine structure parameter. The insert shows a diagram of energy levels for the orientation $B \parallel c$, the circles show the populations of energy levels, conditionally corresponding to the Boltzmann distribution, the bottom shows EPR transitions at low temperatures, the intensities reflect the populations of levels for $D > 0$. Figure 2, *b* shows the orientation dependence of the EPR spectra of ions Mo^{4+} in 6*H*-SiC *n*-type crystal, sample No 2, registered at lower temperature of 1.8 K. As a result, the influence of the Boltzmann distribution on

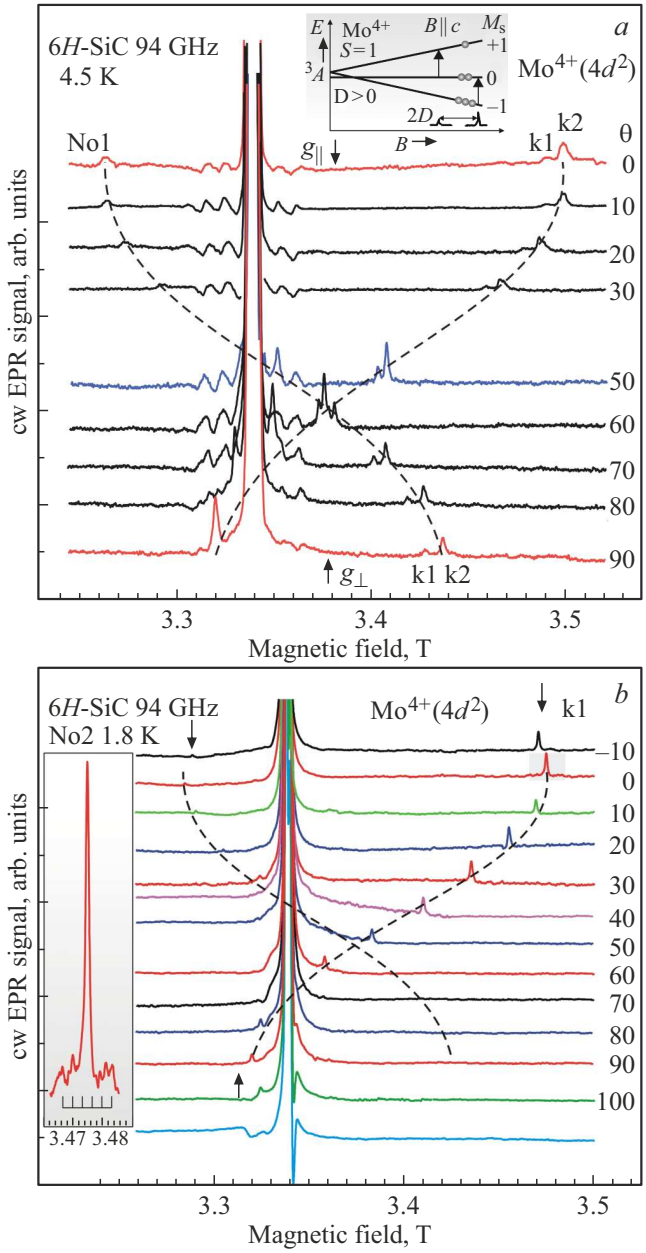

Figure 2. (*a*) Orientation dependence of spectraof EPR ions $Mo^{4+}(4d^2)$ with spin $S = 1$ in compensated crystal 6*H*-SiC, registered in sample No 1 at 4.5 K in range 94 GHz, low frequency modulation 680 Hz, modulation amplitude 0.2 mT. In the region $g = 2$ the intense signals of nitrogen donors are observed, as well as a spectrum of ions Mn^{2+}, not related to SiC. The insert shows a diagram of energy levels for the orientation $B \parallel c$, the circles conditionally show the populations of energy levels in accordance with Boltzmann distribution, the bottom shows EPR transitions at low temperatures, the intensities conditionally reflect the populations of levels for $D > 0$. (*b*) Orientation dependence of EPR spectra of ions Mo^{4+} in crystal 6*H*-SiC of *n*-type, sample No 2, registered at temperature 1.8 K. The insert shows high-field EPR line for orientation close to $B \parallel c$, for which HF structure is visible from interaction with nuclei of odd molybdenum isotopes ^{95}Mo (15.9%, $\mu_I \sim -0.910\,\mu_N$, $I = 5/2$) and ^{97}Mo (9.6%, $\mu_I = -0.929\,\mu_N$, $I = 5/2$), μ_N — nuclear magneton.

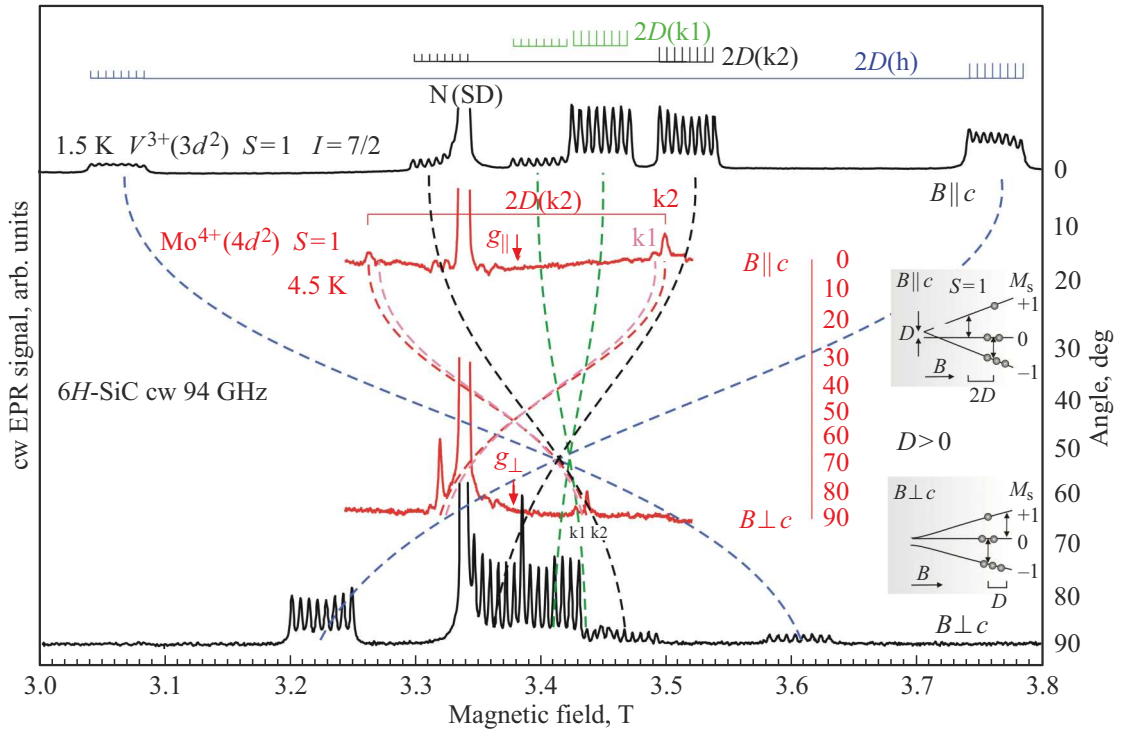

Figure 3. EPR spectra and their orientation dependences in the 6*H*-SiC crystal, registered in continuous mode at frequency of 94 GHz, for Mo^{4+} (4.5 K) and V^{3+} (1.5 K) with isoelectronic configurations $4d^2$ and $3d^2$, respectively, characterized by the triplet state $S = 1$. ESR spectra are presented for two orientations $B \parallel c$ and $B \perp c$. For ions V^{3+} ESR spectra are observed for the three crystalline positions available in 6*H*-SiC (see Figure 1), for ions Mo^{4+} EPR spectra were recorded in two quasi-cubic positions only. For vanadium ions the HF structure is observed determined by the presence of one isotope ^{51}V, content 100%, nuclear spin $I = 7/2$. The inserts schematically show energy levels for the triplet state in two orientations $B \parallel c$ and $B \perp c$, conditionally showing ESR transitions and distribution of level populations in accordance with the Boltzmann distribution at low temperatures and strong magnetic fields. On the right there are scales for the angles between the symmetry axis of paramagnetic centers, coinciding with the hexagonal axis c of the crystal, and the direction of the magnetic field.

the intensity of two EPR lines for low-field and high-field transitions is more clearly manifested (see the level diagram in Figure 2, *a*). The insert shows high-field EPR line for orientation close to $B \parallel c$, for which HF structure is visible from interaction with nuclei of odd isotopes of molybdenum ^{95}Mo (15.9%, $\mu_{I\sim} = -0.910\,\mu_N$, $I = 5/2$) and ^{97}Mo (9.6%, $\mu_I = -0.929\,\mu_N$, $I = 5/2$), μ_N — nuclear magneton.

The spin Hamiltonian describing the EPR spectra of ions Mo^{4+} has the form

$$\hat{H} = \mu_B g_{\|} B_z \hat{S}_z + \mu_B g_{\perp}(B_x \hat{S}_x + B_x \hat{S}_x) + D[\hat{S}_z^2 - (1/3)S(S+1)] + \mathbf{S}\cdot\mathbf{A}\cdot\mathbf{I}, \qquad (1)$$

where z — direction of axis c. The first two terms represent the anisotropic Zeeman interaction. The third term describes the fine structure, where the parameter D is a measure of the axial crystal field acting on the ion $Mo^{4+}(4d^2)$ and explains the characteristic angular dependence of EPR signals of molybdenum during rotation of the magnetic field B from $B \parallel c$ to $B \perp c$. The last term in (1) describes the HF interaction, which is realized only for odd isotopes ^{95}Mo and ^{97}Mo, which have a non-zero magnetic moment with nuclear spin $I = 5/2$ for both isotopes.

As mentioned above, the point group symmetry for all three positions is — C_{3v}, but these positions differ significantly in the axial crystal field, the magnitude of which follows the ratio k1 < k2 < h. This leads to different parameters D for ions Mo^{4+} occupying different positions, and the ratio (for absolute values) $D(k1) < D(k2) < D(h)$ is realized. It is believed that EPR spectra Mo^{4+} are observed in two quasicubic positions (k1, k2). The large ionic radius of Mo atoms, as well as due to the close electronegativity values of Si and Mo, suggests a substituting Si — position for Mo in SiC. The weaker intensity of EPR line at k1 position is caused by the influence of the position of the Fermi level.

Solving the spin Hamiltonian (1), taking into account the term describing the HF interaction, gives the following parameters for $Mo^{4+}(4d^2)$ in two positions in 6*H*-SiC crystal: $D(k1) = 109.3\,mT = 3.06\,GHz$, $D(k2) = 117.5\,mT = 3.29\,GHz$. Measurements of g-factors in the high-frequency range lead to the values $g_{\|} = 1.9787$ and $g_{\perp} = 1.9811$, i.e. $g_{\perp} > g_{\|}$ (in our earlier publication

on the results of measurements in X-range [1] the inverse ratio for g-factors was given). HF structure for the isotopes ^{95}Mo and ^{97}Mo is not resolved in the EPR spectra due to the close values of their nuclear magnetic moments and the relatively large width of the EPR lines. Estimates show that for ^{95}Mo $A_{\|} \sim A_{\perp} = 3.3$ mT.

It is interesting to compare the fine structure parameters for isoelectronic configurations nd^2. Figure 3 shows EPR spectra and their orientation dependences in 6H-SiC crystal, registered in continuous mode at frequency of 94 GHz, for Mo^{4+} (4.5 K) and V^{3+} (1.5 K) [21] with isoelectronic configurations $4d^2$ and $3d^2$, respectively, characterized by triplet state $S = 1$. ESR spectra are presented for two orientations $B \parallel c$ and $B \perp c$. For ions V^{3+} EPR spectra are observed for three crystalline positions available in 6H-SiC (see Figure 1), for ions Mo^{4+} EPR spectra were recorded in two quasi-cubic positions only. For vanadium ions the HF structure is observed determined by the presence of one isotope ^{51}V, content 100%, nuclear spin $I = 7/2$. The inserts schematically show energy levels for the triplet state in two orientations $B \parallel c$ and $B \perp c$, conditionally showing ESR transitions and distribution of level populations in accordance with the Boltzmann distribution at low temperatures and strong magnetic fields. On the right there are scales for the angles between the symmetry axis of paramagnetic centers, coinciding with the hexagonal axis c of the crystal, and the direction of the magnetic field. It can be seen that for quasi-cubic positions the fine structure splittings are close in magnitude and are characterized by positive values of the parameter D.

3.1.2. Optically detectable EPR

Figure 4, a shows MCD absorption spectra for $Mo^{4+}(4d^2)$ ions in the near-IR region in compensated 6H-SiC crystal, sample No 1 (upper two spectra), registered at two temperatures 1.5 and 50 K, and in 6H-SiC n-type crystal with high content of nitrogen donors, sample No 2 (lower spectrum). Strong MCD absorption is observed in the spectral range 1.10−1.25 eV with several sharp zero-phonon lines (ZPLs). MCD absorption of all these ZPLs ia strong diamagnetic part prevails, and the weak paramagnetic part can be used for ODMR experiments.

The paramagnetic part of MCD absorption represents the ground state magnetization of the impurity center, resulting from the Boltzmann distribution of spin level populations. If a change is introduced into the aforementioned distribution as a result of resonant absorption of microwave energy under EPR conditions, the EPR of the ground state of the impurity center can be detected optically by change in the associated MCD absorption spectrum, i. e., one of the ODMR diagrams can be performed.

In accordance with the selection rules for circularly polarized electric dipole transitions in the magnetic field, MCD absorption signal consists of two parts:

$$E = E_p(P) + E_d(B_0),$$

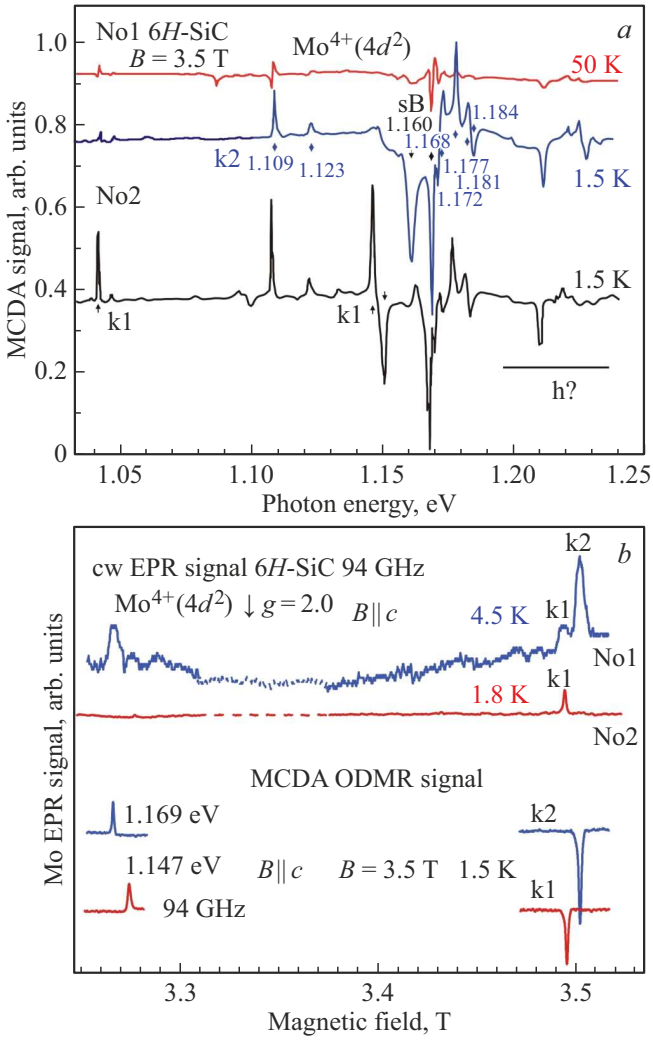

Figure 4. (a) MCD absorption spectra for $Mo^{4+}(4d^2)$ ions in the near IR region in compensated 6H-SiC crystal, sample No 1 (upper two spectra) registered at two temperatures 1.5 and 50 K, and in 6H-SiC n-type crystal with high content of nitrogen donors, sample No 2 (lower spectrum). The correspondence of zero-phonon absorption lines to nonequivalent lattice sites in 6H-SiC was established on the basis of ODMR results. (b) EPR spectra for two samples Nos 1 and 2, recorded at frequency of 94 GHz in the orientation $B \parallel c$, taken from Figure 2, a and b (upper two spectra) and ODMR spectra registered from changes in MCD absorption on the zero-phonon lines 1.147 and 1.169 eV (lower two spectra). Only spectra $Mo^{4+}(4d^2)$ located at the quasicubic lattice sites k1 and k2 are observed.

where E_p — the paramagnetic part, depending on the spin polarization P of the ground state, and E_d — diamagnetic part, proportional to B_0 and arising due to unresolved Zeeman splittings in optically excited states. To register EPR the paramagnetic part is used only. For $S = 1/2$ we get

$$E_p(P) \propto P = (n_- - n_+)/(n_- + n_+) = \tanh(g_e\mu_B/2kT). \quad (2)$$

For $S > 1/2$ P is determined by the Brillouin function. The paramagnetic part E_p depends on temperature and magnetic field according to (2). Measuring E_p as a function of temperature, it can be distinguished from non-magnetic circular dichroism of the sample, since E_d is independent of temperature. The principle of detecting MCD absorption by the EPR method follows from expression (2). The equilibrium spin polarization of the ground state P can be changed by microwave-induced magnetic dipole transitions provided that the transition rate exceeds the spin-lattice relaxation rate, and the light intensity is weak enough so that the optical transitions do not have a noticeable effect on the populations. Microwave resonant EPR transitions reduce E_p, this leads to change in MCD absorption, i. e., to optical detection of EPR. Theoretically, it is possible to obtain 100% effect if EPR transition is completely saturated, i. e. $n_+ = n_-$.

In the case of $Mo^{4+}(4d^2)$ the MCD absorption splitting for different crystal positions is apparently smaller than the spin-orbit splitting (~ 55 meV). Therefore, groups of MCD absorption lines represent a superposition of the spectra of ions Mo^{4+} occupying positions k1, k2 and h in 6H-SiC lattice (see Figure 1). The correspondence of zero-phonon absorption lines to nonequivalent lattice sites in 6H-SiC was established on the basis of ODMR results. Figure 4, b shows EPR spectra for two samples Nos 1 and 2, recorded at frequency of 2 GHz in the orientation $B \parallel c$, taken from Figure 2, a and b (upper two spectra) and ODMR spectra registered from changes in MCD absorption on the zero-phonon lines 1.169 and 1.147 eV (lower two spectra). Only spectra $Mo^{4+}(4d^2)$ located at the quasicubic lattice sites k1 and k2 are observed.

The calculation diagram of $Mo^{4+}(4d^2)$ in 6H-SiC is shown in Figure 5. Term for the free ion $Mo^{4+}(4d^2)$ ^3F (orbital moment $L = 3$, spin $S = 1$, state with 24-fold degeneracy, 7-fold in orbital moment and 3-fold in spin) is split as a result of interaction with the cubic crystal field $H_{cub}(T_d)$ into three levels: an orbital singlet $^3A_2$, and two orbital triplets $^3T_2$ and $^3T_1$, as shown in the diagram, which also shows the orbital and spin degeneracy of the levels. The following excited states of the free ion are significantly higher than the term ^3F, so they can not be considered as a source of optical transitions. The observed MCD absorption occurs from the ground state $^3A_2$ to the first excited state $^3T_2$, the levels of which are split due to the spin-orbit interaction H_{SO}, and the influence of the trigonal crystal field $H_{trig}(C_{3v})$. The splitting $^3T_2$ by spin-orbit interaction is ~ 55 meV, while trigonal splitting increases the spectral extent of the spin-orbit multiplet. The splitting of individual levels by trigonal field, shown in Figure 5, is assessed qualitatively based on group-theoretical considerations. While the trigonal splitting in the multiplet $^3T_2$ is resolved optically, the splitting of the ground state $^3A_2$ is so small that it falls within the line width of the optical transitions. The splitting of the term $^3A_2$ is identical to the splitting D of the triplet spin multiplet determined from ODMR and EPR experiments, and is

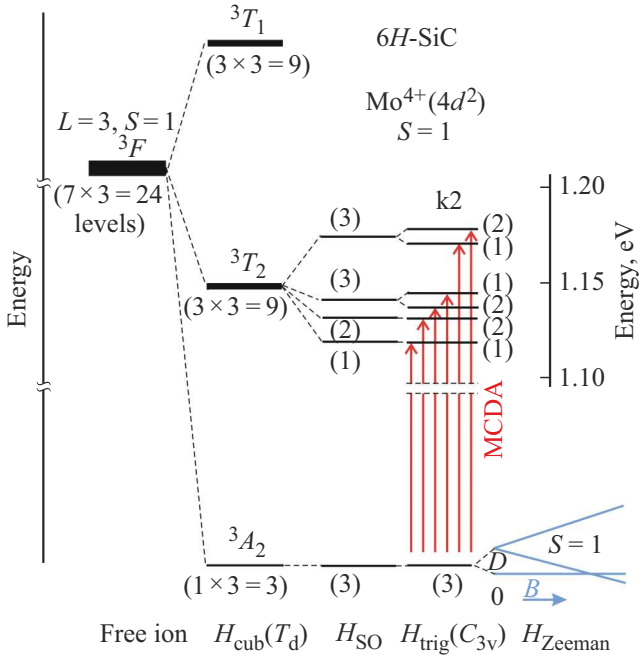

Figure 5. Calculation diagram $Mo^{4+}(4d^2)$ in 6H-SiC. Term for the free ion $Mo^{4+}(4d^2)$ ^3F (orbital moment $L = 3$, spin $S = 1$, state with 24-fold degeneracy, 7-fold in orbital moment and 3-fold in spin) is split as a result of interaction with the cubic crystal field H_{cub} (symmetry T_d) into three degenerate levels $^3A_2$, $^3T_2$ and $^3T_1$, as shown in the diagram, which also shows the orbital and spin degeneracy of the levels. The observed MCD absorption occurs from the ground state $^3A_2$ to the first excited state $^3T_2$, the levels of which are split due to the spin-orbit interaction H_{SO}, and the influence of the trigonal crystal field H_{trig} (symmetry C_{3v}). The splitting of the spin-orbit levels of the state $^3T_2$ by the trigonal field is indicated only qualitatively; however, it is resolved in the optical absorption spectra, at that the splitting of the ground state is significantly less than the width of the optical absorption line. However, their magnitude and sign are determined from a comparison of the ODMR and EPR spectra. In the geometry of the MCD absorption experiment, six polarization transitions $E \perp c$ are observed.

$\sim 0.1\,cm^{-1}$. It arises only due to a small admixture of excited states $^3T_2$ and $^3T_1$ [6] as a result of spin-orbit interaction. In the geometry of the MCD absorption experiment six polarization transitions $E \perp c$ are observed, which are assigned to $Mo^{4+}(4d^2)$, since ODMR Mo^{4+} is observed if the registration system is configured to any of these lines.

EPR spectrum $Mo^{4+}(4d^2)$ can also be detected in the commercial material of bulk plate 6H-SiC, i. e. It is obvious that molybdenum is a trace impurity in SiC. The concentration of $Mo^{4+}(4d^2)$ in sample No 1 lies in the range $10^{15}\,cm^{-3}$, while the concentration of Mo in sample No 2 is by at least an order of magnitude smaller. EP spectrum $Mo^{4+}(4d^2)$ was not observed in the bulk material of the plate 6H-SiC of p-type, sample No 3. The MCD absorption technique turned out to be extremely sensitive. For bulk

crystals the degree of detection Mo^{4+} is within $10^{13}\,cm^{-3}$. Trace impurities Mo^{4+} can be detected in thin layers up to thicknesses of several micron.

3.2. Molybdenum $Mo^{5+}(4d^1)$

Figure 6 shows the orientation dependence of EPR spectra of $Mo^{5+}(4d^1)$ ions registered in X-range at temperature of 15K in 6H-SiC sample of p-type, No 3. These spectra are described by the spin Hamiltonian (1) for $S = 1/2$ (in this case, of course, the terms describing the fine structure are omitted). EPR spectrum is presented for a perpendicular orientation of the magnetic field. EPR linewidth is extremely small, which made it possible to separate two odd isotopes Mo (^{95}Mo, ^{97}Mo). The angular dependence of HF structure is shown by points in Figure 6 for the isotope ^{95}Mo. For a more accurate description of the orientation dependences of HF structure, it is necessary to add to the above spin Hamiltonian the additional expression $Q[I_{Z^2} - (l/3)I(l+l)]$, which describes the quadrupole interaction, mainly with the quadrupole moment of the isotope ^{97}Mo (quadrupole moment of the isotope ^{97}Mo in absolute value is approximately by order of magnitude greater than the quadrupole moment of the isotope ^{95}Mo), where Q is a measure of the interaction of the quadrupole moment of the corresponding isotope with the electric field gradient at the location of the ion Mo^{5+} [6]. The influence of the electric quadrupole moment leads to destruction of the equidistance HF structure lines and causes additional „forbidden" transitions.

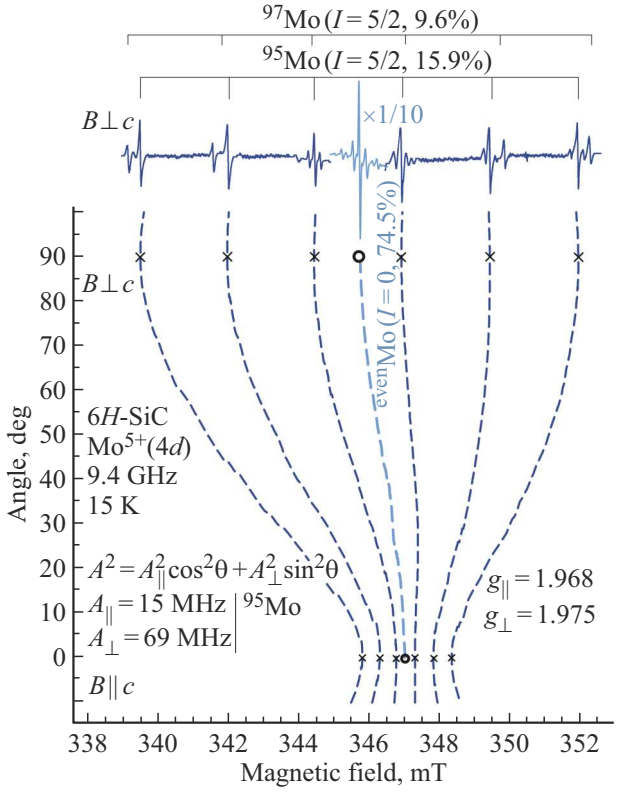

Figure 6. Orientation dependence of EPR spectra of $Mo^{5+}(4d^1)$ ions registered in X-range at temperature of 15 K.

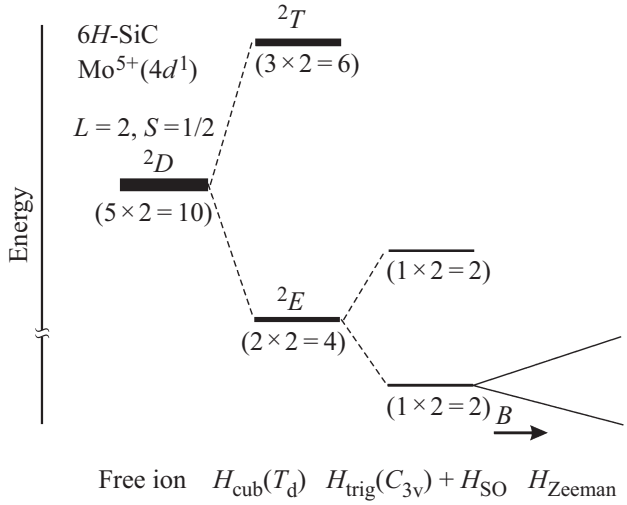

Figure 7. Splitting of one-electron energy levels of 4d-orbital under the influence of crystal field and spin-orbit coupling. In free atom five orbitals corresponding to 4d-shell (not considering spin), degenerated. The crystal field of cubic symmetry breaks this degeneracy, creating an orbital triplet and a doublet, while the crystal field of symmetry C_{3v} (trigonal) splits the five orbitals into one singlet and two doublets. The spin-orbit interaction is responsible for the doublets splitting, generating in total five sets of Kramers doublets considering the electron spin. The energy splittings caused by the magnetic field inside these Kramers doublets lead to the introduction of parameters of spin Hamiltonian with effective spin $S' = 1/2$.

The spin Hamiltonian (1) solution gives the following parameters: $g_{\|} = 1.968$, $g_{\perp} = 1.975$; $A_{\perp} = 23.0 \cdot 10^{-4}\,cm^{-1}$ and $A_{\|} = 5 \cdot 10^{-4}\,cm^{-1}$ for isotope ^{95}Mo and $A_{\perp} = 23.5 \cdot 10^{-4}\,cm^{-1}$, $A_{\|} = 4 \cdot 10^{-4}\,cm^{-1}$ and $Q = 2.9 \cdot 10^{-4}\,cm^{-1}$ for isotope ^{97}Mo. Ratio of constants of HF structures of two Mo isotopes for perpendicular orientation $(A_{\perp}(^{95}\text{Mo})/A_{\perp}(^{97}\text{Mo}) = 0.979)$ is exactly equal to ratio of their nuclear magnetic moments $(\mu(^{95}\text{Mo})/\mu(^{97}\text{Mo}) = 0.979)$, this is unambiguous evidence of chemical identity of Mo centers. Another independent evidence of the chemical nature of Mo centers is the relative intensity of the HF structure 15.3% (^{95}Mo) and 7.8% (^{97}Mo), which exactly corresponds to natural content of these Mo isotopes.

Figure 7 schematically shows the splitting of one-electron energy levels of 4d-orbital under the action of crystal field and spin-orbit interaction [6]. Term for free ion $Mo^{5+}(4d^1)$ ^{2}D ($L = 2$, $S = 1/2$), five orbitals corresponding to 4d-shell (not considering spin), degenerated. The crystal field of cubic symmetry (T_d) breaks this degeneracy, producing orbital triplet ^2T and doublet ^2E, while trigonal crystal field of symmetry C_{3v} and spin-orbit interaction leads to further splitting, generating a set of Kramers doublets considering the electron spin. The energy splittings caused by the magnetic field inside these Kramers doublets lead

to the introduction of parameters of spin Hamiltonian with effective spin $S' = 1/2$.

Figure 8 shows the analysis of SHF structure observed in EPR spectrum of Mo^{5+} ions in 6*H*-SiC, due to interaction with ^{29}Si and nuclei ^{13}C. A transition is presented for even isotopes of molybdenum with zero magnetic moment, i. e., without HF splitting, while the SHF interaction with the ligand nuclei is clearly observed. The dashed line shows one of HF transitions for ^{95}Mo isotope with magnification x27 (the magnification value was chosen taking into account the natural content of isotopes and six HF components for ^{95}Mo isotope), central line of which is artificially combined with the transition for even isotopes of molybdenum. To explain this structure a non-central position of Mo^{5+} ion in the silicon site of 6*H*-SiC crystal is assumed, as shown schematically in Figure 8, *b*. Only twelve silicon atoms in the second coordination sphere are shown, the interaction with them is analyzed in Figure 8, *a*. Simulation of EPR spectrum gives the following parameters of SHF structure for Mo^{5+} in the silicon site of 6*H*-SiC crystal: SHF interaction (i) with three equivalent atoms of silicon No 1−3 is 27 MHz; (ii) with six atoms of silicon N No 4−9 is 10.4 MHz; (iii) with three atoms of silicon No 10−12 is 4.2 MHz. The natural content of ^{29}Si isotope, which has a nuclear magnetic moment with $I = 1/2$, is 4.7%. If there are N equivalent silicon atoms near Mo^{5+} ion in silicon site, the probability of finding one nucleus of ^{29}Si isotope increases by N times. It should be noted that the SHF interaction with the nuclei of silicon atoms is assumed to be isotropic. The four nearest carbon atoms, located in the first coordination sphere relative to Mo^{5+} ion, and with which SHF interaction is supposed, are not indicated in the diagram. Simulation of EPR spectrum gives the splitting of SHF structure for Mo^{5+} in the silicon site for interaction with carbon atoms 37.1 MHz in the magnetic field orientation perpendicular to the axis *c*, with which the axial symmetry of the center coincides Mo^{5+} in the silicon site.

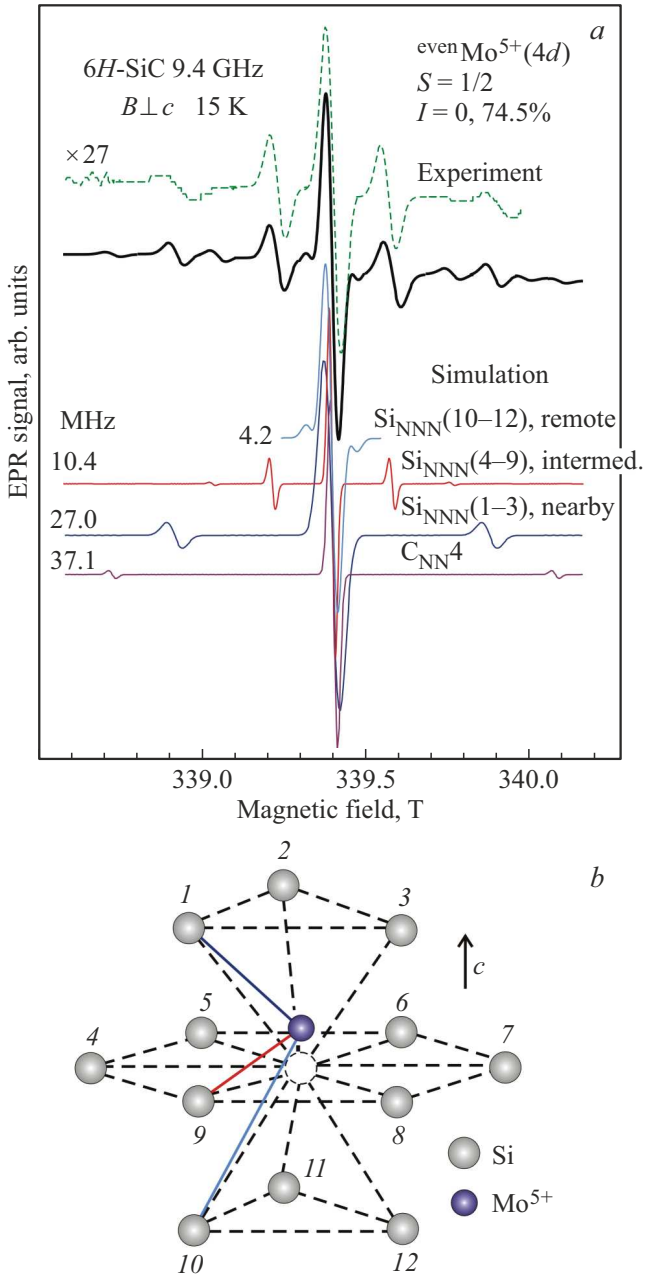

Figure 8. (*a*) Analysis of SHF structure observed in EPR spectrum of Mo^{5+} ions in 6*H*-SiC, due to interaction With ^{29}Si and ^{13}C nuclei. A transition is presented for even isotopes of molybdenum with zero magnetic moment, i. e., without HF splitting, while the SHF interaction with the ligand nuclei is clearly observed. The dashed line shows one of HF transitions for ^{95}Mo isotope with magnification x27 (the magnification value was chosen taking into account the natural content of isotopes and six HF components for ^{95}Mo isotope), central line of which is artificially combined with the transition for even isotopes of molybdenum. (*b*) The expected non-central position of Mo^{5+} ion in the silicon site of 6*H*-SiC crystal. Only twelve silicon atoms in the second coordination sphere are shown, the interaction with them is shown in Figure 8, *a*. The four nearest carbon atoms, located in the first coordination sphere relative to Mo^{5+} ion, and with which SHF interaction is supposed, are not indicated in the diagram.

3.3. Molybdenum $Mo^{3+}(4d^3)$

In crystal 6*H*-SiC of *n*-type, sample No 2, together with above described EPR signals of Mo^{4+} ions, the additional EPR lines are observed, they differ by strong angular dependence [1]. The angular dependence of this signal corresponds to a center with fictitious spin $S' = 1/2$ and highly anisotropic factor g', and is described by the expression $g'^2 = g'^2_{\parallel} \cos^2\theta + g'^2_{\perp} \sin^2\theta$, where θ denotes the angle between constant magnetic field B and the hexagonal axis *c* of the crystal. Analysis of experimental data gives the following parameters: $g'_{\parallel} = 1.945$, $g'_{\perp} = 3.939$.

HF structure from odd isotopes of molybdenum unambiguously identifies the center as belonging to molybdenum. EPR spectrum of the molybdenum state $Mo^{3+}(4d^3)$ is observed only in 6*H*-SiC crystals of *n*-type with high content of nitrogen donors. EPR spectrum of $Mo^{3+}(4d^3)$ ions can be described by the spin Hamiltonian (1) for $S = 3/2$. Under

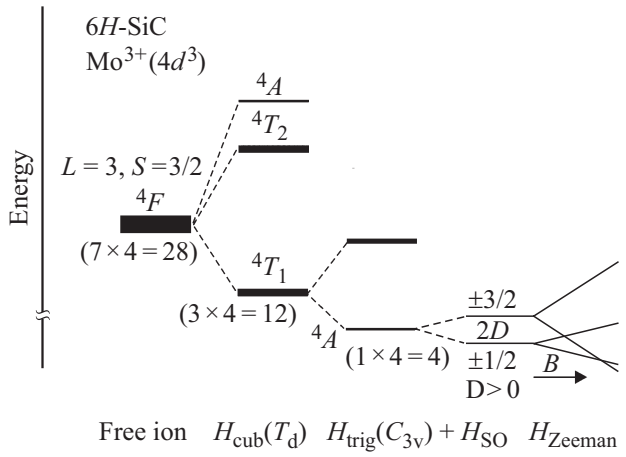

Figure 9. Diagram for energy levels of $Mo^{3+}(4d^3)$ ion in 6*H*-SiC. The term for free ion $Mo^{3+}(4d^3)$ ^4F (orbital moment $L = 3$, spin $S = 3/2$, state with 28-fold degeneracy, 7-fold in orbital moments and 4-fold in spin) is split as result of interaction with cubic crystal field H_{cub} (symmetry T_d) to three degenerate levels $^4T_1$, $^4T_2$ and ^4A, as shown in the diagram, which also shows the orbital and spin degeneracy of the levels. The lower state levels $^4T_1$ are split due to the spin-orbit interaction H_{SO} and the influence of the trigonal crystal field H_{trig} (symmetry C_{3v}).

conditions of large values of $|D|$, significantly exceeding the microwave quantum, the lower Kramers doublet can be considered as state having an effective spin $S' = 1/2$. In this case, for state with effective spin $S' = 1/2$ we can use the relations $g'_{\|} = g_{\|}$, $g'_{\perp} = 2g_{\perp}\{1 - (3/16)(h\nu/2D)^2\}$, $A'_{\|} = A_{\|}$, $A'_{\perp} = 2A_{\perp}\{1 - (3/16)(h\nu/2D)^2\}$. Thus, the angular dependence of EPR signal of Mo^{3+} is characterized by highly anisotropic effective g'-factor with values given above. The angular dependence of EPR of $Mo^{3+}(4d^3)$ is completely similar to the angular dependence of EPR of $Cr^{3+}(3d^3)$ [1,7].

The diagram for the energy levels of the $Mo^{3+}(4d^3)$ ion in 6*H*-SiC is shown in Figure 9. Term for the free ion $Mo^{3+}(4d^3)$ ^4F(orbital moment $L = 3$, spin $S = 3/2$, state with 28-fold degeneracy, 7-fold in orbital moment and 4-fold in spin) is split as a result of interaction with the cubic crystal field H_{cub} (symmetry T_d) into three degenerate levels $^4T_1$, $^4T_2$ and ^4A, as shown in the diagram, which also shows the orbital and spin degeneracy of the levels. The lower state levels $^4T_1$ are split due to the spin-orbit interaction H_{SO} and the influence of the trigonal crystal field H_{trig} (symmetry C_{3v}). Note that till now it was possible to detect EPR $Mo^{3+}(4d^3)$ only for one of the three lattice sites in 6*H*-SiC.

There is interest in comparison of the HF structure observed for all three charge states of molybdenum. Figure 10 shows positions of HF components for interaction With nuclei of two odd isotopes ^{95}Mo (15.9%) and ^{97}Mo (9.6%), $I = 5/2$, for three charge states of molybdenum in 6*H*-SiC: (*a*) Mo^{3+}, (*b*) Mo^{4+} and (*c*) Mo^{5+}. HF structure of two isotopes is allowed for Mo^{5+} ions only. HF interaction for ions Mo^{3+} and Mo^{4+} is practically isotropic and is determined mainly by the polarization of the inner *s*-shells due to interaction with unpaired 4*d*-electrons, while the HF interaction for ions Mo^{5+}, which have one unpaired 4*d*-electron, is characterized by strong anisotropy. Figure 10, *c* shows EPR spectrum registered in orientation

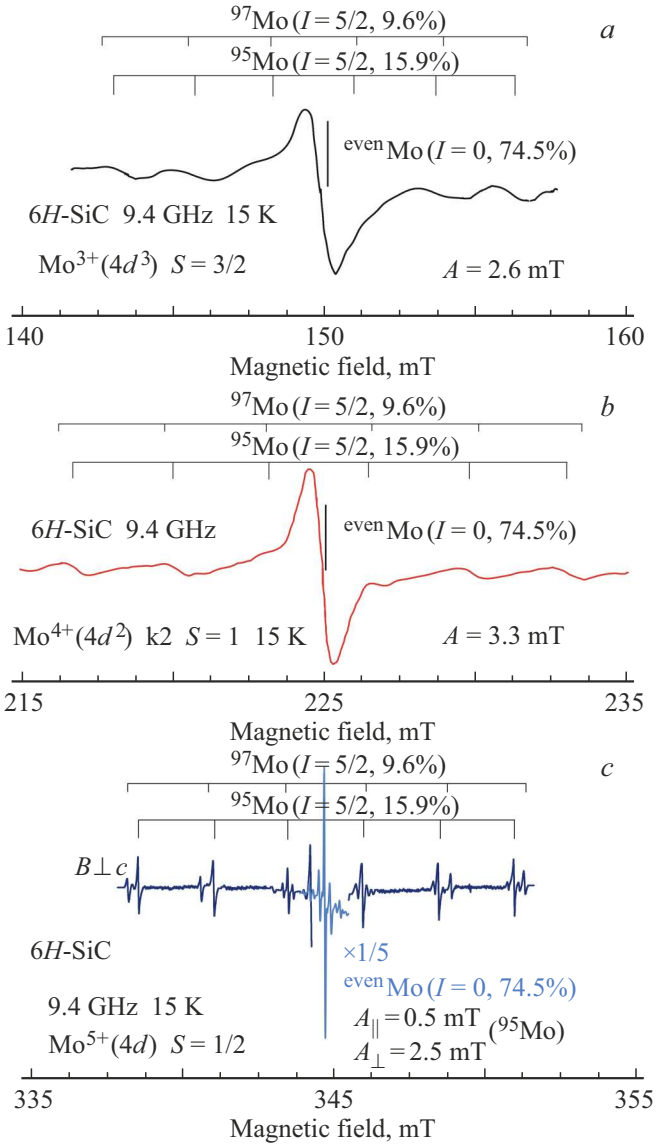

Figure 10. Relative positions of HF component of interaction With nuclei of two odd isotopes ^{95}Mo (15.9%) and ^{97}Mo (9.6%), $I = 5/2$, for three charge states of molybdenum in 6*H*-SiC (*a*) Mo^{3+}, (*b*) Mo^{4+} and (*c*) Mo^{5+}. HF structure of two isotopes is allowed for Mo^{5+} ions only. HF interaction for ions Mo^{3+} and Mo^{4+} is practically isotropic and is determined mainly by the polarization of the inner *s*-shells due to interaction with unpaired 4*d*-electrons, while the HF interaction for ions Mo^{5+}, which have one unpaired 4*d*-electron, is characterized by strong anisotropy, Figure 10, *c* shows EPR spectrum registered in $B \perp c$ orientation is shown. The central single line in all three spectra refers to the nuclei of even molybdenum isotopes that do not have nuclear magnetic moment ($I = 0$).

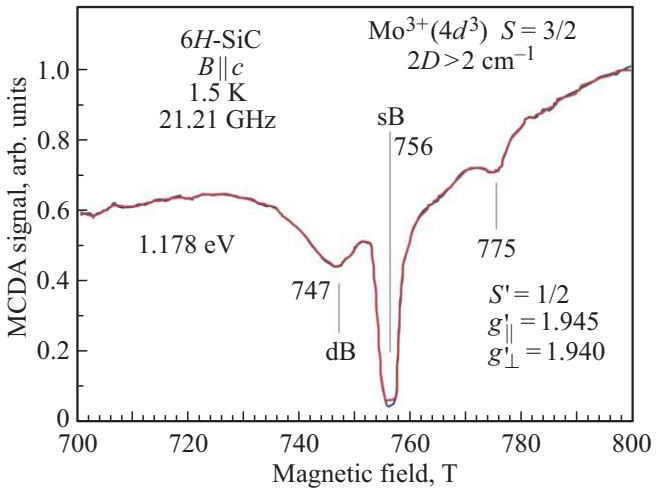

Figure 11. ODMR signal at $g_{\|} = 1.944$ is observed together with strong resonance Mo^{4+}. Comparison with conventional EPR shows that this resonance belongs to $Mo^{3+}(4d^3)$ ions. Also in the center in the region $g = 2$ one can see ODMR signal of the shallow acceptor B (sB) and the signal of the deep boron acceptor (dB) at $g_{\|} = 2.026$.

$B \perp c$. The central single line in all three spectra refers to the nuclei of even molybdenum isotopes that do not have nuclear magnetic moment ($I = 0$).

Figure 11 shows ODMR signal at $g_{\|} = 1.944$, which is observed together with strong resonance Mo^{4+}. Comparison with conventional EPR shows that this resonance belongs to $Mo^{3+}(4d^3)$ ions. Since this signal appears only as a weak satellite of the resonance Mo^{4+} in MCD absorption experiments, it is probably a background signal that is not directly related to the apparently correlated with Mo^{4+}MCD absorption. Also in the center in the region $g \sim 2$ one can see ODMR signal of the shallow boron acceptor (sB) and the signal of the deep boron acceptor (dB) at $g_{\|} = 2.026$. Note that sB resonance is observed on almost all MCD absorption lines. dB signals are registered only on some of them. These signals are background and probably are due to photoionization of acceptors.

We carried out experiments with high-temperature diffusion of boron into 6*H*-SiC crystals, in which ESR spectra of various charge states of molybdenum described in the previous sections were previously observed. As a result, all EPR spectra associated with molybdenum disappeared, i. e. in crystal heavily doped with an acceptor impurity (*p*-type with high concentration of acceptor impurity) the molybdenum transforms into non-paramagnetic state. Probably, diamagnetic $Mo^{6+}(4d^0)$, inaccessible to EPR, is the thermal equilibrium state of Mo centers in these crystals.

Recent paper [9] studied the optical characteristics of vanadium V^{4+} in silicon carbide for application in quantum information and communication. These defects have narrow lines of optical emission in the telecommunication window near 1300 nm, while the lifetime in the excited state is about 50 ns, and the presence of HF interaction leads to additional splitting of levels that are promising for use in quantum photonic technologies.

Note that at room temperature a significant decrease in PL V^{4+} in silicon carbide is registered. At the same time, in the telecommunications window near 1500 nm erbium Er^{3+} in silicon carbide is very promising. Semiconductors doped with erbium are of great interest due to the existence of electronic transitions inside $4f$-shell $^4I_{13/2} \rightarrow {}^4I_{15/2}$ at wavelength of 1.54 μm, which coincides with the minimum absorption in the fiber optics. In papers [22–25] the problem of introducing an erbium impurity into silicon carbide crystals was solved. As a result, EPR and photoluminescence spectra were observed in the near-IR range in the region of 1.54 μm, unambiguously belonging to Er^{3+} ions, replacing silicon in 6*H*-SiC lattice and located in several positions, like the molybdenum ions shown in Figure 1. In the paper [22] the temperature dependences of the relative intensities of the PL spectra of ions of vanadium V^{4+} and erbium Er^{3+} were measured (Figure 12).

It can be seen that the PL intensity of V^{4+} ions at room temperature drops by more than an order of magnitude

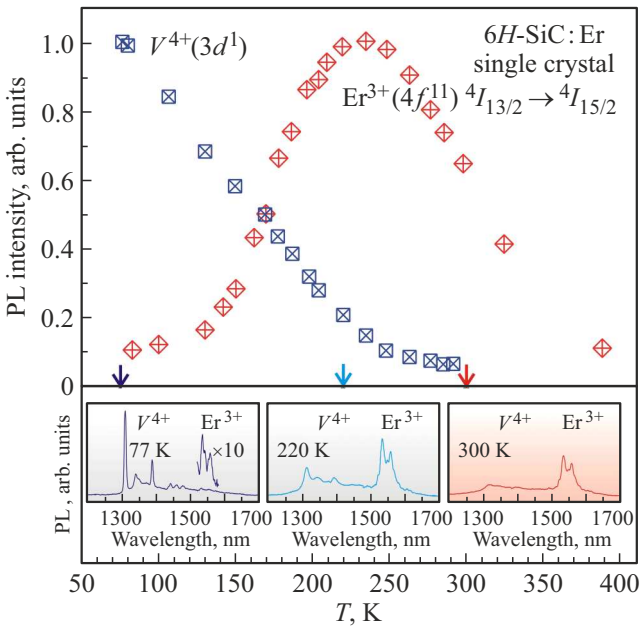

Figure 12. Temperature dependences of PL intensity of vanadium V^{4+} and erbium Er^{3+} ions, which show that the PL intensity of V^{4+} ions decreases at room temperature by more than order of magnitude compared to the PL intensity at 77 K, while the PL intensity of Er^{3+} ions increases by more than order of magnitude with temperature increasing from 77 to 240 K, at which the maximum value is observed PL intensity, with a further increase to room temperature the PL intensity decreases slightly by approximately 30% of the maximum value. The PL spectra of V^{4+} and Er^{3+} at three temperature points are shown, clearly illustrating the relative PL intensities of the mentioned ions. The advantage of erbium ions at room temperature is obvious, the lines are quite narrow, and there are several overlapping PL lines related to different erbium positions in 6*H*-SiC lattice.

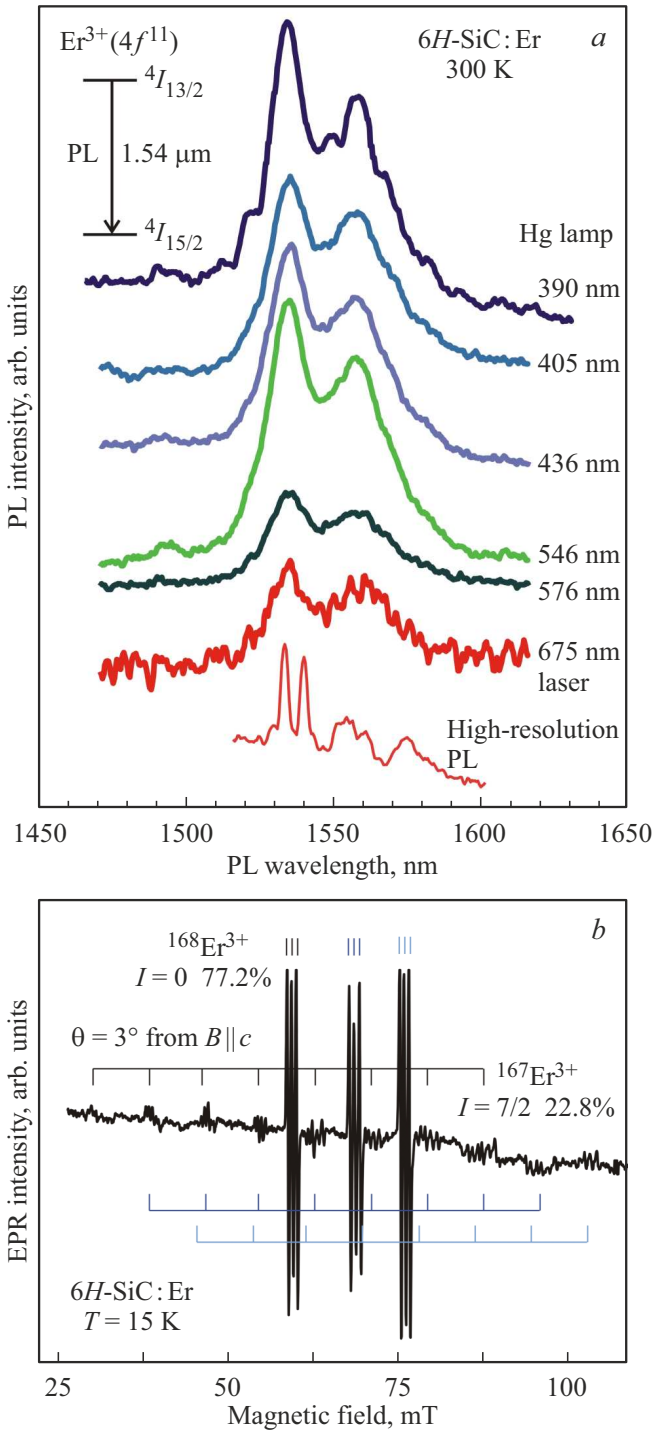

Figure 13. (*a*) PL spectra of Er^{3+} ions in 6*H*-SiC : Er crystal at room temperature, registered at different excitation wavelengths, isolated from the mercury lamp spectrum. Two laser-excited PL spectra are shown below. (*b*) Characteristic EPR spectrum of Er^{3+} ions occupying three positions in the lattice (see Figure 1), registered near the orientation of the magnetic field along the hexagonal axis *c* of crystal. HF structure of eight lines is visible for the odd erbium isotope, which has a nuclear spin $I = 7/2$. The orientation is intentionally turned away from the axis *c* by several degrees so that HF structure packs appear more clearly.

compared to PL intensity at 77 K, while the PL intensity of Er^{3+} ions increases by more than an order of magnitude with temperature increasing from 77 to 240 K, at which the maximum value of PL intensity is observed, with a further increase to room temperature the PL intensity drops slightly by approximately 30% of the maximum value. It is important to emphasize that the PL of Er^{3+} decrease by order of magnitude from the maximum value occurs only at temperature about 400 K. Figure 12 shows PL spectra of V^{4+} and Er^{3+} at three temperature points, clearly illustrating the relative PL intensities of the mentioned ions. The advantage of erbium ions at room temperature is obvious, the lines are quite narrow, and there are several overlapping PL lines related to different erbium positions in 6*H*-SiC lattice. We believe that the use of the optical properties of erbium in silicon carbide is very promising for long-distance optical communications. Taking into account the unique spin properties: the giant electron *g*-factor of Er^{3+} about $g \sim 6$, i. e. strong splitting of Zeeman levels in relatively weak magnetic fields, and the presence of isotope with high nuclear spin, these structures can be promising in quantum communications. As an illustration, Figure 13 shows the characteristic EPR spectrum of Er^{3+} ions occupying three positions in the lattice (see Figure 1), recorded near the orientation of the magnetic field along the hexagonal axis c of the crystal. Erbium has two stable isotopes ^{168}Er, with nuclear spin $I = 0$ and natural content of 77.2% and ^{167}Er, $I = 7/2$, 22.8%. Thus, EPR spectrum shall consist of intense central line due to ^{168}Er even isotope and eight weak lines of HF structure due to the interaction with the nuclear spin of ^{167}Er odd isotope. Figure 13, *b* clearly shows HF structure of eight lines for the erbium odd isotope, which has nuclear spin $I = 7/2$. The orientation is intentionally turned away from the axis *c* by several degrees so that HF structure packs appear more clearly. More detailed studies of EPR and parameters of the spin Hamiltonian for a series of erbium centers Er^{3+} in 6*H*-SiC are given in papers [6,23].

4. Conclusion

Four possible charge states of molybdenum in SiC are analyzed: paramagnetic $Mo^{3+}(4d^3)$, $Mo^{4+}(4d^2)$, $Mo^{5+}(4d^1)$, characterized by axial symmetry, and diamagnetic $Mo^{6+}(4d^0)$. Using high-frequency EPR and low temperatures for Mo^{4+} with spin $S = 1$, which is a neutral charge state in the crystal A^0, a positive sign of fine structure splitting has is established *D* for two quasicubic positions k1 and k2: $D(k1) = 3.06$ GHz, $D(k2) = 3.29$ GHz and values $g_{\|} = 1.9787$ and $g_{\perp} = 1.9811$ are determined, i. e. $g_{\perp} > g_{\|}$. Using MCD absorption methods at different temperatures, the contributions of the paramagnetic and diamagnetic components in the zero-phonon optical absorption lines of Mo^{4+} ions in the near-IR region are separated. For the charge state $Mo^{5+}(4d^1)$, which is of special interest for applications in quantum technologies in connection with

the recent discovery of PL of these ions, the non-central position of the impurity in the silicon site is established, and SHF interactions with ligand nuclei ^{29}Si and ^{13}C were determined. The comparative analysis of HF interactions with odd isotopes of molybdenum ^{95}Mo and ^{97}Mo, which have nuclear magnetic moment, was executed in three charge states. In connection with the occurrence of papers on the use of vanadium V^{4+} in SiC in quantum information and communication, and since these defects have PL lines in the telecommunication window near 1300 nm [16], it is shown that in the main telecommunication window near 1540 nm, erbium Er^{3+} in SiC, which we previously managed to introduce into bulk SiC crystals [22–25], is very promising. It is important that at room temperature there is a significant drop in PL V^{4+} in SiC, while for Er^{3+} ions in SiC such drop is insignificant, and PL can be observed up to 400 K.

Funding

This study was supported by the Russian Science Foundation, project No. 23-12-00152, https://rscf.ru/project/23-12-00152/

Conflict of interest

The authors declare that they have no conflict of interest.

References

[1] K.F. Dombrowski, M. Kunzer, U. Kaufmann, J. Schneider, P.G. Baranov, E.N. Mokhov. Phys. Rev. B **54**, 7323 (1996).
[2] J. Baur, M. Kunzer, K.F. Dombrowskii', U. Kaufmann, J. Schneider, P.G. Baranov, E.N. Mokhov. Identification of multivalent molybdenum impurities in SiC crystals. Inst. Phys. Conf. Ser. No 155. Ch. 12, 933 (1997), IOP Publishing Ltd.
[3] J. Baur, M. Kunzer, K.F. Dombrowski, U. Kaufmann, J. Schneider, P.G. Baranov, E.N. Mokhov. Mater.Sci. Eng. B **46**, 313 (1997).
[4] M. Kunzer, K.F. Dombrowski, F. Fuchs, U. Kaufmann, J. Schneider, P.G. Baranov, E.N. Mokhov. Proc. ISCM '95. Just. Phys. Conf. Ser. **142**, 385 (1996).
[5] P.G. Baranov, I.V. Il'in, E.N. Mokhov, V.A. Khramtsov. Phys. Solid State **41**, 783 (1999).
[6] P.G. Baranov, H.-J. von Bardeleben, F. Jelezko, J. Wrachtrup. Magnetic Resonance of Semiconductors and Their Nanostructures: Basic and Advanced Applications. Springer Series in Materials Science. Springer-Verlag GmbH Austria (2017). V. 253. 539 c.
[7] P.G. Baranov, V.A. Khramtsov, E.N. Mokhov. Semicond. Sci. Technol. **9**, 1340 (1994).
[8] A. Gruber, A. Dräbenstedt, C. Tietz, L. Fleury, J. Wrachtrup, C. von Borczyskowski. Science **276**, 2012 (1997).
[9] P.G. Baranov, I.V. Il'in, E.N. Mokhov, M.V. Muzafarova, S.B. Orlinskii, J. Schmidt. JETP Lett. **82**, 441 (2005).
[10] P.G. Baranov, A.P. Bundakova, I.V. Borovykh, S.B. Orlinskii, R. Zondervan, J. Schmidt. JETP Lett. **86**, 202 (2007).
[11] P.G. Baranov, A.P. Bundakova, A.A. Soltamova, S.B. Orlinskii, I.V. Borovykh, R. Zondervan, R. Verberk, J. Schmidt. Phys. Rev. B **83**, 125203 (2011).
[12] M. Widmann, S.-Y. Lee, T. Rendler, N.T. Son, H. Fedder, S. Paik, L.-P. Yang, N. Zhao, S. Yang, I. Booker, A. Denisenko, M. Jamali, S. Ali Momenzadeh, I. Gerhardt, T. Ohshima, A. Gali, E. Janzén, J. Wrachtrup. Nature Mater. **14**, 164 (2015).
[13] D.J. Christle, A.L. Falk, P. Andrich, P.V. Klimov, J.U. Hassan, N.T. Son, E. Janzén, T. Ohshima, D.D. Awschalom. Nature Mater. **14**, 160 (2015).
[14] W.F. Koehl, B. Diler, S.J. Whiteley, A. Bourassa, N.T. Son, E. Janzén, D.D. Awschalom. Phys. Rev. B **95**, 035207 (2017).
[15] B. Diler, S.J. Whiteley, C.P. Anderson, G. Wolfowicz, M.E. Wesson, E.S. Bielejec, F.J. Heremans, D. Awschalom. npj Quantum Inform. **6**, 11 (2020).
[16] G. Wolfowicz, C.P. Anderson, B. Diler, O.G. Poluektov, F.J. Heremans, D.D. Awschalom. Sci. Adv. **6**, 18 (2020).
[17] T. Bosma, G.J.J. Lof, C.M. Gilardoni, O.V. Zwier, F. Hendriks, B. Magnusson, A. Ellison, A. Gällström, I.G. Ivanov, N.T. Son, R.W.A. Havenith, C.H. van der Wal. npj Quantum Inform. **4**, 48 (2018).
[18] N.G. Romanov, V.V. Dyakonov, V.A. Vetrov, P.G. Baranov. FTT **31**, 106 (1989) (in Russian).
[19] P.G. Baranov, V.V. Dyakonov, N.G. Romanov, V.A. Vetrov. Phys. Status Solidi B **159**, K33 (1990).
[20] F.I. Ahlers, P.G. Baranov, N.G. Romanov , I.M. Shpat. FTT **30**, 427 (1988). (in Russian)
[21] E.V. Edinach, A.D. Krivoruchko, A.S. Gurin, M.V. Muzafarova, I.V. Ilyin, R.A. Babunts, N.G. Romanov, A.G. Badalyan, P.G. Baranov. FTP, **54**, 103 (2020). (in Russian).
[22] R.A. Babunts, V.A. Vetrov, I.V. Il'in, E.N. Mokhov, N.G. Romanov, V.A. Khramtsov, P.G. Baranov. Phys. Solid State **42**, *5*, 829 (2000).
[23] P.G. Baranov, I.V. Ilyin, E.N. Mokhov. Solid State Commun. **103**, 291 (1997).
[24] P.G. Baranov, I.V. Il'in, E.N. Mokhov, V.A. Khramtsov. Phys. Solid State **41**, 783 (1999).
[25] G. Baranov, I.V. Il'in, E.N. Mokhov, A.B. Pevtsov, V.A. Khramtsov. Phys. Solid State **41**, 32 (1999).

Translated by I.Mazurov